Introducing Ion Mobility Mass Spectrometry to Identify Site-Selective C-H Bond Activation in N-Heterocyclic Carbene Metal Complexes

Andrés Mollar-Cuni,[a] Laura Ibáñez-Ibáñez,[a] Gregorio Guisado-Barrios[b] , Jose A. Mata[a] and Cristian Vicent[*c]

[a]Institute of Advanced Materials (INAM), Centro de Innovación en Química Avanzada (ORFEO-CINQA), Universitat Jaume I, Avda. Sos Baynat s/n, 12071, Castellón (Spain).
[b]Departamento de Química Inorgánica. Instituto de Síntesis Química y Catálisis Homogénea (ISQCH), CSIC-Universidad de Zaragoza, 50009, Zaragoza (Spain).
[c]Serveis Centrals d'Intrumentació Científica (SCIC). Universitat Jaume I, Avda. Sos Baynat s/n, 12071, Castellón (Spain). E-mail: barrera@uji.es

Abstract

The activation of C-H bonds in a selective manner still constitutes a major challenge from the synthetical point of view, thus it remains as an active area of fundamental and applied research. Herein, we introduce Ion Mobility Spectrometry Mass Spectrometry-based (IM-MS) approaches to uncover site-selective C-H bond activation in a series of metal complexes of general formula $[(NHC)LMCl]^+$ (NHC = N-Heterocyclic carbene; L = pentamethylcyclopentadiene (Cp*) or p-cymene; M = Pd, Ru and Ir). The C-H bond activation at the N-bound groups of the NHC ligand is promoted upon Collision Induced Dissociation (CID). The identification of the resulting $[(NHC - H)LM]^+$ isomers relies on the distinctive topology that such cyclometalated isomers adopt upon site-selective C-H bond activation. Such topological differences can be reliably evidenced as different mobility peaks in their respective CID-IM mass spectra. Alternative isomers are also identified via dehydrogenation at the Cp*/p-cymene (L) ligands to afford $[(NHC)(L – H)M]^+$. The fragmentation of the ion mobility-resolved peaks is also investigated by CID-IM-CID. It enables the assignment of mobility peaks to the specific isomers formed from $C(sp^2)$-H or $C(sp^3)$-H bond activation and distinguishes them from the Cp*/p-cymene (L) dehydrogenation isomers. The conformational change of the NHC ligands upon C-H bond activation, concomitant with cyclometallation, is also discussed on the basis of the estimated Collision Cross Section (CCS). A unique conformation change of the pyrene-tagged NHC members is identified that involves the reorientation of the NHC ring accompanied by a folding of the pyrene moiety.

Introduction

Cyclometalation constitutes one of the mildest metal-mediated activation of unreactive bonds, especially for C(sp2)-H or C(sp3)-H bonds.[1–4] A wide range of ligands are prone to form cyclometalated complexes, including N-Heterocyclic Carbenes (NHCs).[5–7] Due to their strong *σ*-donation capability, they are excellent candidates to facilitate intramolecular C-H bond activation processes involving their N-bound substituents, eventually leading to cyclometalated species. C-H activation in NHCs has enormous implications for catalysis. For instance, cyclometalated NHC complexes of Pd, Ru, Co, Rh, Ir are efficient catalysts in transfer hydrogenation, amidation, oxidation of alcohols or tandem oxidation / Wittig /reduction processes.[6–13] They also display unique reactivity patterns; for example, as intermediates in the direct functionalization of azolium salts for the synthesis of functionalized molecules,[14–17] or in the preparation of complexes containing ruthenium-element (E = Si, Ge, Sn) multiple bonds.[18,19] Still, a major challenge in C-H bond activation is the ability to differentiate (and activate) highly similar C-H bonds in a target molecule. In the case of cyclometalated NHCs, subtle modifications in the NHC backbone, the solvent medium and/or the metal precursor may lead to site-selective C-H activation sites upon metal coordination.[20] The NHC cyclometalated complexes derived thereof display distinctive physico-chemical features that are known to substantially alter their intrinsic catalytic activity.[21–24]

The mechanistic picture of the above-mentioned transformations is often triggered by an intramolecular C-H activation in the N-bound groups of the NHC. Such C-H bond activation is frequently found to be a reversible process and produce highly reactive and/or short lived cyclometalated intermediates.[25–33] Despite having a comprehensive mechanistic proposal is crucial to success, the identification of the site-selective C-H bond activation in these NHC complexes may become challenging using NMR or X-ray diffraction methods. In this context, soft ionization Mass spectrometry (MS) techniques, such as Electrospray Ionization (ESI), and its tandem version are commonly used to uncover speciation and mechanistic insights in catalysis.[34–42] However, MS detection itself does not provide structural and conformational information about the isomers resulting from competitive C-H activation unless selective deuteration is achieved (a task difficult to achieve).[43] We envisioned that Ion Mobility Spectrometry Mass Spectrometry (IM-MS) could serve to identify these isomers as long as site-selective C-H bond activation affords isomeric products of different topology (size and shape). Until now, IM-MS has facilitated the identification of mixtures of isomers on a wide spectrum of compounds based on their distinctive Collision Cross Section (CCS), which can be correlated with their size and shapes.[44,45] In the case of gas-phase ion chemistry studies, the use of the IM-MS technique was pioneered in 2011,[46,47] and it has also been used to study the structural and

conformational analysis of Ru/arene complexes,[48–50] and to differentiate the topology of organometallic gyroscope-like complexes.[51] Mechanistic studies that rely on the use of IM-MS are also documented,[52–56] although the technique is rarely used. In this context, we have foreseen that it could potentially be used to identify the cyclometalated products resulting from site-selective C-H bond activation, since to the best of our knowledge it remains unexplored.

Herein we investigated the C-H activation of a series of NHC based metal complexes of general formula $[(NHC^{1\text{-}4})LMCl]^+$ (NHC^n = N-Heterocyclic carbene ligands where 1: R = R' = 3,4,5-trimethoxybenzyl; 2: R = Me, R' = Pyr; 3: R = R' = Me ; 4: R = Mes, R' = Pyr; L = pentamethylcyclopentadiene (Cp*) or p-cymene; M = Pd, Ru and Ir) displayed in Chart 1 using IM-MS methods. The NHC ligands bound to Pd, Ru and Ir encompass both symmetrical and unsymmetrical NHC ligands, two halides and one additional (pyridine, Cp* or p-cymene) ligand. The unsymmetrical NHC ligands bear different N-bound groups both of them amenable to be involved in intramolecular C-H bond activation processes.

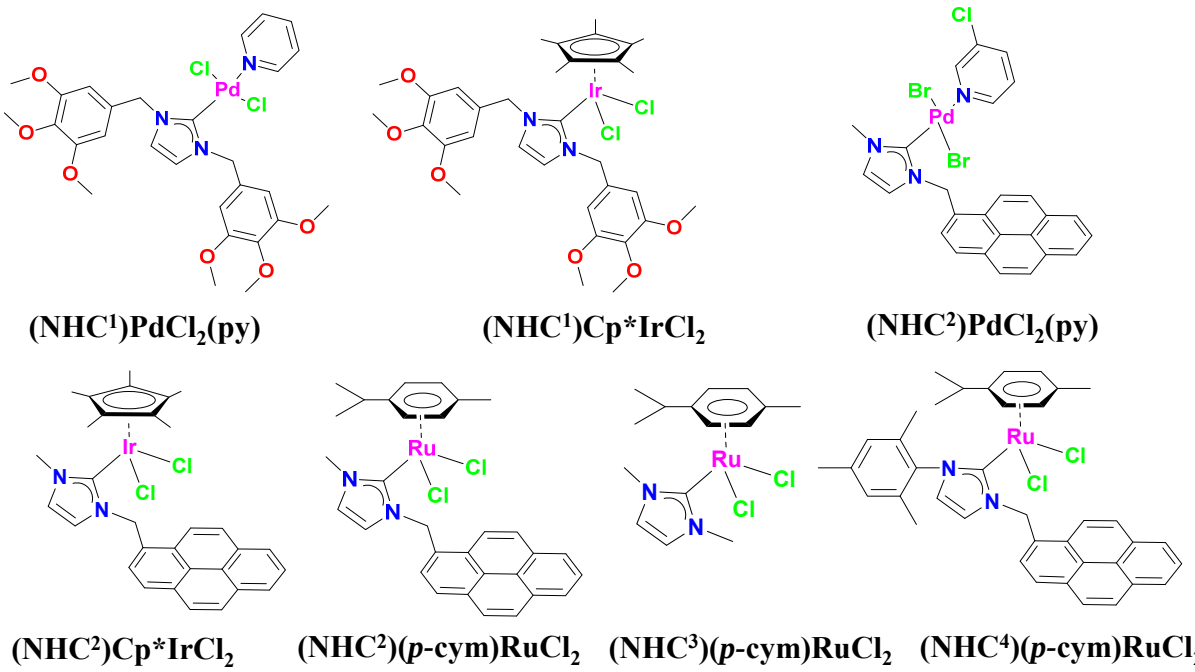

Chart 1. Schematic representation of the NHC based Ir, Pd and Ru complexes

Results and dicussion

The compounds shown in Chart 1 were investigated by Electrospray Ionization (ESI), Collision Induced Dissociation (CID) and Ion Mobility Spectrometry Mass Spectrometry (IM-MS). These dihalide complexes are gently transferred to the gas-phase upon ESI via loss of a first halide ligand (see equation 1).[57] Hence, the ESI mass spectra of Ir and Ru compounds displayed the corresponding $[(NHC^n)Cp^*IrCl]^+$ or $[(NHC^n)(p\text{-cym})RuCl]^+$ cations as the base peak. In the case

of the Pd PEPPSI type complexes,[58] besides halide release, the loss of the pyridine ligand also takes place to produce the $[(NHC^n)PdX]^+$ (Cl or Br) cations as the base peak.

$(\mathbf{NHC^n})LM\mathbf{Cl}_2$	$\rightarrow [(\mathbf{NHC^n})LM\mathbf{Cl}]^+ + Cl^-$	(equation 1)
$[(\mathbf{NHC^n})LM\mathbf{Cl}]^+$	$\rightarrow [(\mathbf{NHC^n} - H)LM]^+ + HCl$	(equation 2)
$[(\mathbf{NHC^n} - H)LM]^+$	→ second-generation product ions	(equation 3)

The intramolecular C-H bond activation is triggered upon Collision Induced Dissociation (CID) involving the second halide ligand and the reactive C-H site (see equation 2) concomitant with the liberation of HCl. Such transformation is reminiscent to the dehydrochlorination procedure occurring in solution to access Ru-based cyclometalated NHC complexes via C-H bond activation.[18,28] Numerous studies also exploit the HCl release upon CID conditions as a means to promote C-H bond activation and explore its mechanism in detail in a well-defined gas-phase environment.[59–64] In the present work, CID experiments were performed upon mass-selection of the species of interest in the first quadrupole, subjected to CID fragmentation followed by ion mobility separation aimed at identifying potential cyclometalated isomers (see equation 2). Complementary CID experiments registered after the ion mobility separation were also performed as a means to obtain structural information of the ion mobility-resolved isomers (see equation 3). In this mode of operation, the precursor ion of interest is selected with the quadrupole mass filter, subjected to CID fragmentation followed by ion mobility separation. Next, ion mobility-resolved isomers are subjected to a second fragmentation step in a second collision cell. Hence, second-generation product ions are detected that can help to the structural assignment of the isomers. Additional experimental details are given in the Experimental Section and Schemes S1-S3 in the Supporting information.

Initially, we evaluated the C-H bond activation of two distinct metal complexes bearing the symmetrical NHC^1 ligand (1: R = R'= 3,4,5-trimethoxybenzyl) (Chart 1). CID mass spectra followed by ion mobility separation of $[(NHC^1)PdCl]^+$ (*m/z* 567.0) and $[(NHC^1)Cp^*IrCl]^+$ (*m/z* 789.2) are shown in Figure 1 a) and b), respectively together with the arrival time distribution (ATD) of the product ions. In both cases, the exclusive dehydrochlorination is clearly evidenced as a neutral loss of HCl (Δm 36) upon CID conditions.

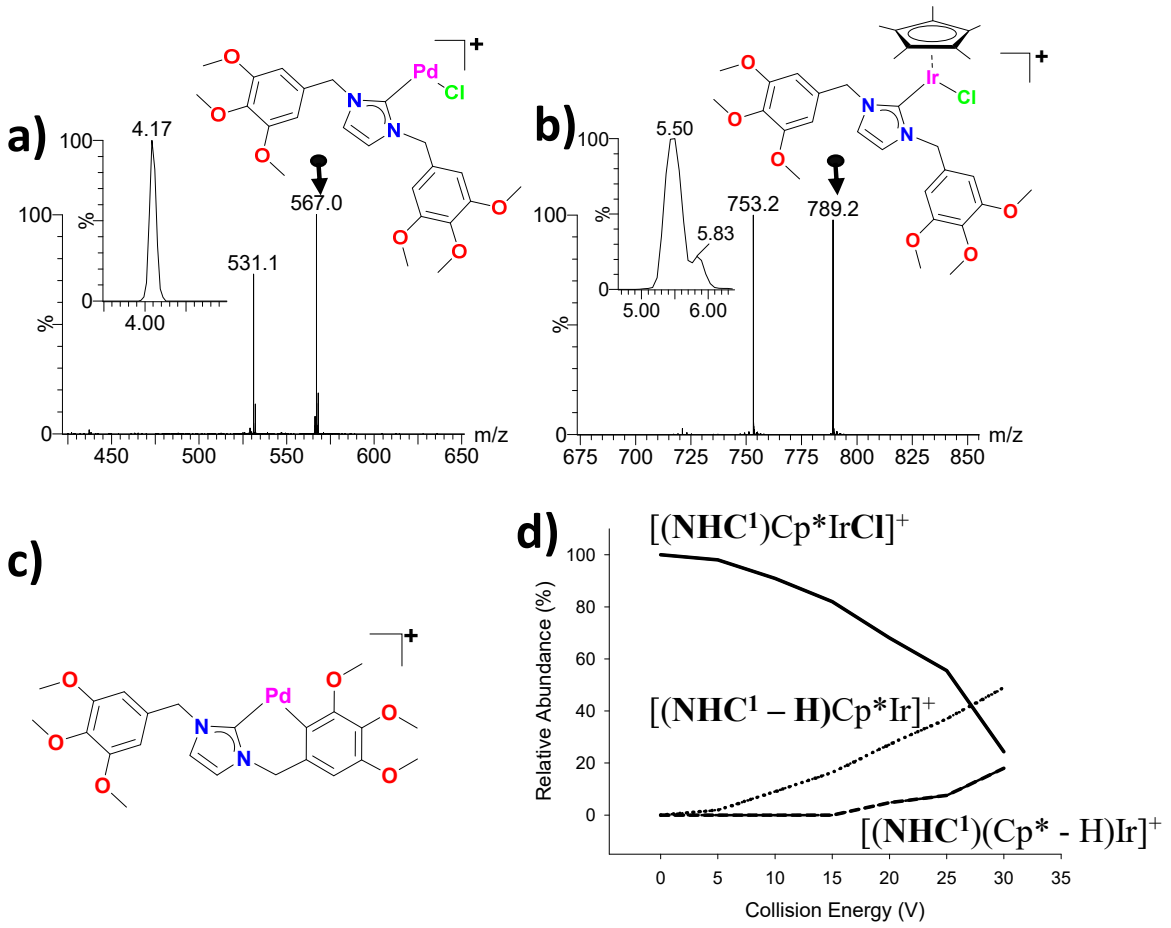

Fig. 1. CID mass spectra of a) $[(NHC^1)PdCl]^+$ (*m/z* 567.0) and b) $[(NHC^1)Cp^*IrCl]^+$ (*m/z* 789.2) registered at a collision energy of 25 V along with the arrival time distributions (ATDs) of the product ions; c) proposed cyclometalated ligand arrangement in the $[(NHC^1 – H)Pd]^+$ cation (also applicable to the related Ir $[(NHC^1 – H)Cp^*Ir]^+$ member; d) breakdown profile of the precursor $[(NHC^1)Cp^*IrCl]^+$ (*m/z* 789.2) ion showing the contribution of both $[(NHC^1 - H)Cp^*Ir]^+$ and $[(NHC^1)(Cp^* - H)Ir]^+$ isomers extracted from the areas of their mobility peaks.

For the palladium $[(NHC^1)PdCl]^+$ (*m/z* 567.0) complex, its product ion at *m/z* 531.1 displays a single gaussian-shaped mobility peak in its ATD (see inset in Figure, 1a), suggesting the presence of a single and energetically-favored isomer. The occurrence of multiple C-H activation processes is clearly ruled out due to the symmetric nature of the NHC^1 ligand. A plausible cyclometalated arrangement is depicted in figure 1c through ortho-metalation concomitant with the formation of a six-membered metalacycle. With regards to the iridium complex $[(NHC^1)Cp^*IrCl]^+$ at *m/z* 789.2, its CID mass spectrum is shown in Figure 1 b) together with the arrival time distribution of the product ion (*m/z* 753.2). At low collision energy (below CE = 25 V; data not shown), the product ion at *m/z* 753.2 displayed a single gaussian-shaped mobility peak at 5.50 ms. A second mobility peak in its ATD profile is observed at 5.83 ms at higher

collision energy (CE = 25 V) (as illustrated in the inset in Figure 1 b)). Besides cyclometalation of the NHC ligand, as in the case of the palladium $[(NHC^1)PdCl]^+$ congener, C-H activation of the Cp* ligand is feasible and both processes could be differentiated by IM-MS. The gas-phase dehydrogenation of the Cp* ligand is precedented in related complexes and it is typically found at harsh fragmentation conditions. It proceeds via deprotonation of a methyl group at the Cp* ligand accompanied by a loss of the chloride ligand leading to a product ion with a η^4-tetramethylfulvene ligand [65–67]and the Ir metal in the oxidation state +I. An schematic representation of both $[(NHC^1 - H)Cp^*Ir]^+$ and $[(NHC^1)(Cp^* - H)Ir]^+$ isomers is given in Figure S1. Further structural insights on the ion mobility-resolved isomers, namely $[(NHC^1 – H)Cp^*Ir]^+$ or $[(NHC^1)(Cp^* - H)Ir]^+$, were gathered from fragmentation studies in the second collision cell. Thus, we obtained second-generation fragments characteristic of each isomer (see figure S2). The isomer that displays the fastest drift time at 5.50 ms presents a product ion at *m/z* 505.1 that is associated to the disruption of the symmetrical NHC ligand. This disruption proceeds via loss of a R'-NHC neutral fragment (R´= 3,4,5-trimethoxybenzyl) leaving the remaining 3,4,5-trimethoxybenzyl group still cyclometalated to the Cp*Ir fragment and is consistent with the assignment of the isomer $[(NHC^1 – H)Cp^*Ir]^+$ to the mobility peak at 5.50 ms. The slowest drifting ion at 5.83 ms displayed a poorer fragmentation pattern (a minor loss of H_2), thus lacking structural information. Breakdown profile graphics represents the relative abundance of the precursor and product ions as the collision energy is increased in a controlled manner. Figure 1 d) shows the breakdown profile the $[(NHC^1)Cp^*IrCl]^+$ cation, taking into account the relative intensity of the precursor and product ions. As different isomeric product ions were identified by CID and IM-MS, the branching ratio of each isomer, namely $[(NHC^1 - H)Cp^*Ir]^+$ or $[(NHC^1)(Cp^* - H)Ir]^+$ was extracted from the relative areas of their mobility peaks at 5.50 ms and 5.83 m, respectively. Such representation is useful to get decoupled insights on the kinetic barrier to trigger site-selective C-H bond activation at the NHC ligand versus Cp* dehydrogenation, otherwise inaccessible by CID experiments in the absence of IM separation. From a perusal of figure 1d) it can be observed that the kinetic barrier for the C-H bond activation at the NHC ligand is lower than the one observed for the dehydrogenation of the Cp* ligand.

Next, we investigated the C-H bond activation of the ions $[(NHC^2)Cp^*IrCl]^+$, $[(NHC^2)(p\text{-cym})RuCl]^+$ and $[(NHC^2)PdBr]^+$, all of them featuring the same pyrene-tagged NHC^2 ligand (2: R = Me, R'= Pyr). The CID mass spectrum of the $[(NHC^2)Cp^*IrCl]^+$ cation at low collision energy resulted in the product ion at *m/z* 621.2 (loss of one HCl molecule) that displayed a single gaussian-shaped mobility peak (see figure 2 a). This observation points towards a selective C-H activation from the pyrene group likely at the ortho position (see inset in Figure 2 a). This hypothesis is confirmed by inspecting the IM-MS of the authentic Ir cyclometalated complex at

the pyrene group, namely [(NHC^2 - H)Cp*IrCl],[68] whose ATD of the ESI-generated [(NHC^2 - H)Cp*Ir]$^+$ cation matches that of the product ion generated from the [(NHC^2)Cp*IrCl]$^+$ cation (see figure S3). At higher collision energy, a second ATD profile is evidenced as a barely visible shoulder with reduced drift time (note the assymetric shape of the mobility peak at 4.64 ms) that we attribute to the Cp* dehydrogenation as we have previously evidenced in the case of complex [(NHC^1)Cp*IrCl$_2$]. Its breakdown representation (see figure S4) points that C-H activation from the NHC^2 ligand is accomplished at lower collision energies that those seen for the NHC^1 ligand, thus suggesting a lower kinetic barrier associated to NHC^2 vs NHC^1 metalation. This also correlates with the observed tendency of the pyrene C(sp2)-H bond to spontaneously metalate in solution. We observed that ESI-MS and NMR monitoring of methanol solutions of [(NHC^2)Cp*IrCl$_2$] leds to the quantitative formation of [(NHC^2 - H)Cp*IrCl] after several hours.

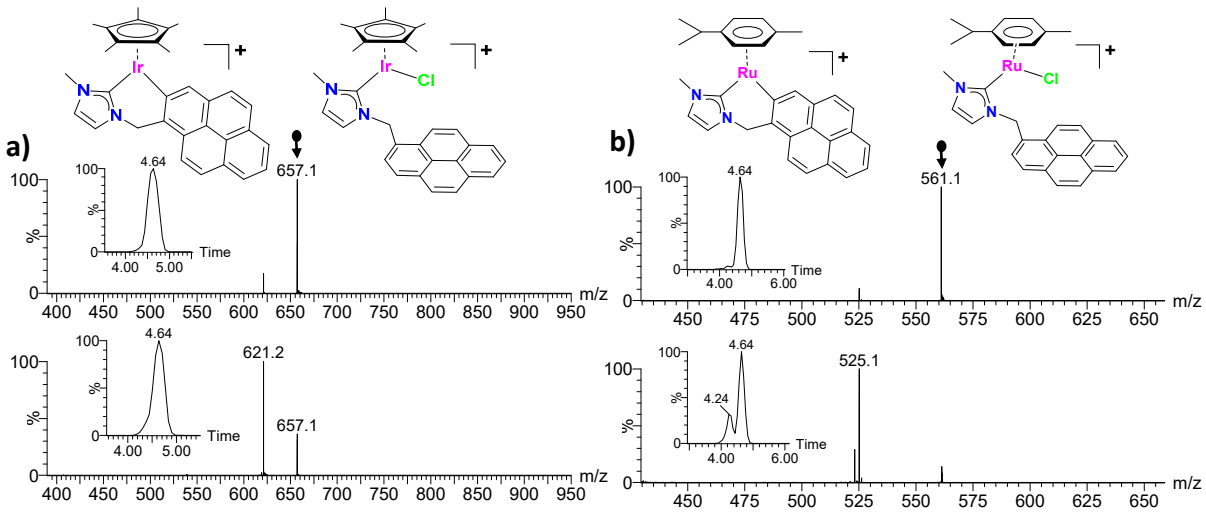

Fig. 2 a) CID mass spectra of [(NHC^2)Cp*IrCl]$^+$ (*m/z* 657.1) and b) [(NHC^2)(p-cym)RuCl]$^+$ (*m/z* 561.1 along with the ATDs (arrival time distributions) for the product ions recorded at 10 V (top) and 20 V (bottom).

Likewise, the product ion at m/z 525.1 that comes from the precursor for [(NHC^2)(p-cym)RuCl]$^+$ (*m/z* 561.1) ion displays a single mobility peak at 4.64 ms at low collision energies associated to the C-H activation from the pyrene group (see figure 2 b). At higher collision energy, a second mobility peak at 4.24 ms is evidenced in its corresponding ATD to the gas-phase dehydrogenation of p-cymene into p,α-dimethylstyrene, a well-documented gas-phase behavior for Ru/p-cymene complexes.[48] Further evidence of the high collision energy associated to the p-cymene dehydrogenation was given by inspection of the CID mass spectra of the cation [(NHC^3)(p-cym)RuCl]$^+$ (see Chart 1). This cation is used as a model because it lacks of N-bound

groups prone to be metalated and the only viable C-H activation process is p-cymene dehydrogenation. Detailed breakdown profiles and CID mass spectra are given in figures S4 and confirm that p-cymene dehydrogenation occurs at high collision energies. For the $[(NHC^2)PdBr]^+$ cation, lacking Cp* or p-cymene ligands, the product ion that results from the HBr loss, namely $[(NHC^2 - H)Pd]^+$ (see figure S6), displayed a single gaussian-shaped mobility peak associated to the C-H activation from the pyrene group in a similar way that found for its Ir and Ru congeners.

Then, we investigated the C-H bond activation at the NHC^4 ligand (4: R = Mes, R' = Pyr). In this case, the $[(NHC^4)(p\text{-cym})RuCl]^+$ ion displays a NHC ligand with different N-bound groups, namely pyrene or mesityl, amenable to trigger both C-(sp2)H and C(sp3)-H bond activation, respectively Either ortho-metalation or alkylmetalation are well-documented cyclometalation reactions observed for Ru.[30] The CID mass spectrum of the precursor $[(NHC^4)(p\text{-cym})RuCl]^+$ ion is shown in Figure 3.

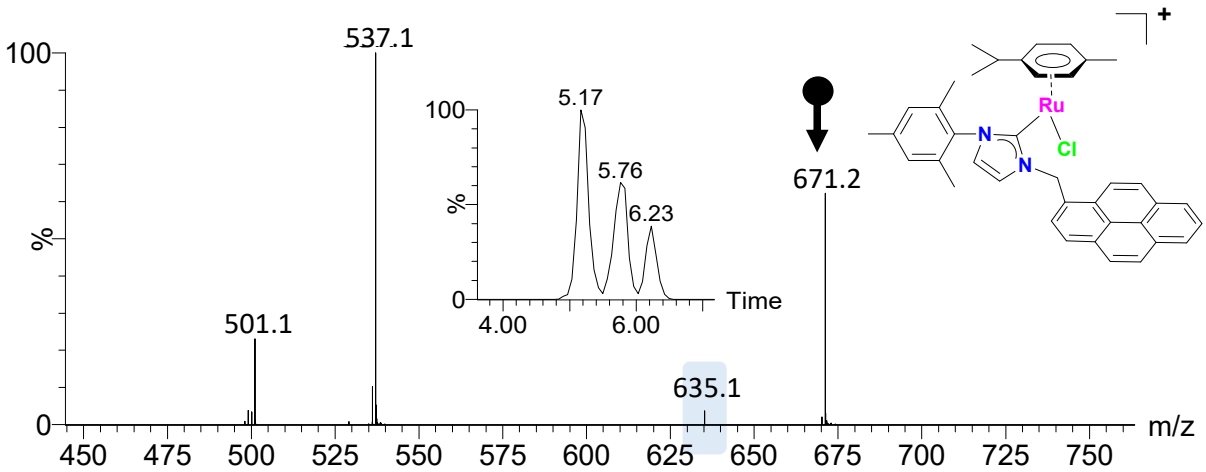

Fig. 3 a) CID mass spectrum of $[(NHC^4)(p\text{-cym})RuCl]^+$ (*m/z* 671.2) at 25 V; blue background is given to the product ions at *m/z* 635.1 that is formed via HCl liberation; the inset shows its ATD highlighting the occurrence of three mobility peaks that supports the formation of up to three isomers.

In this particular case, the dehydrochlorination dissociation pathway (loss of one HCl molecule Δm 36) was minor with respect to a second fragmentation step that involves the p-cymene liberation (Δm 134). A third product ion at *m/z* 501.1 that results from the dehydrochlorination and p-cymene liberation (Δm = 170) is also evidenced. Such p-cymene liberation was not observed in the previous examples (neither for $[(NHC^2)(p\text{-cym})RuCl]^+$ nor $[(NHC^3)(p\text{-cym})RuCl]^+$ complexes) and we hypothesized that the bulky nature of the NHC^4 ligand facilitates the Ru-p-cymene bond dissociation. Nonetheless, the ATD distribution of the dehydrochlorination product ion at *m/z* 635.1 does reveal the occurrence of the three site-

selective C-H bond activation steps as evidenced clearly by three mobility peaks centered at 5.17, 5.76 and 6.23 ms (see inset in figure 3) in its ATD profile. Following the separation in the ion mobility section, these ion mobility-resolved isomers were subjected to fragmentation providing second-generation product ions. Such fragmentation studies gave crucial structural information to propose a tentative assignment of the three isomers. As can be inferred from figure 4 b) and c), the isomers associated to the mobility peaks centered at 5.17 and 5.76 ms display a characteristic loss of p-cymene (Δm 134), thus pointing that both isomers still preserve the p-cymene ligand and should result from the competitive C-(sp2)-H or C(sp3)-H bond activation from the N-bound groups in the NHC^4 ligand. Besides the loss of p-cymene, the isomer attributed to the mobility peak at 5.76 ms (see figure 4 c)) also presents a loss of the Mesityl-NHC group to produce a second-generation product ion at *m/z* 449.1 that still keeps the p-cymene and the metalated pyrene group. The formation of the product ion at m/z 449.1 requires that a hydrogen transfer from the methylene group to the nitrogen of NHC to form the neutral Mesityl-NHC molecule concomitant with the product ion depicted in figure 4 which presumably features two metalated moieties. Such second-generation product ion is absent in the fragmentation of the isomer that displays the mobility peak at 5.17 ms that only presents a dominant p-cymene liberation fragmentation channel at identical fragmentation condtitions. This experiment strongly suggests that the isomer associated to the C(sp2)-H bond activation (from the pyrene group) is that linked to the mobility peak at 5.76 ms whereas the isomer that results from the intramolecular C(sp3)-H bond activation (from the mesityl group) is attributed to the mobility peaks at 5.17 ms. Conversely, the isomer associated to the mobility peak at 6.23 ms does not display p-cymene liberation and it is observed predominantly at higher collision energies. It was attributed to the $[(NHC^4)(p\text{-cym - H})Ru]^+$ isomer following our previous observation on the intrinsic higher collision energy required to promote dehydrogenation from Cp* and p-cymene ligands. Second-generation product ions due to losses of Δm 2 (m/z 633.1) and Δm 132 (m/z 503.1) are observed upon CID conditions (see figure 4 d). The product ion at m/z 633.1 is presumably formed through and additional p-cymene dehydrogenation (Δm 2) whereas the product ion at m/z 503 formally corresponds to the release of p,α-dimethylstyrene (Δm 132) which could be formed via hydride transfer from the (p-cym – H) ligand to the Ru center.

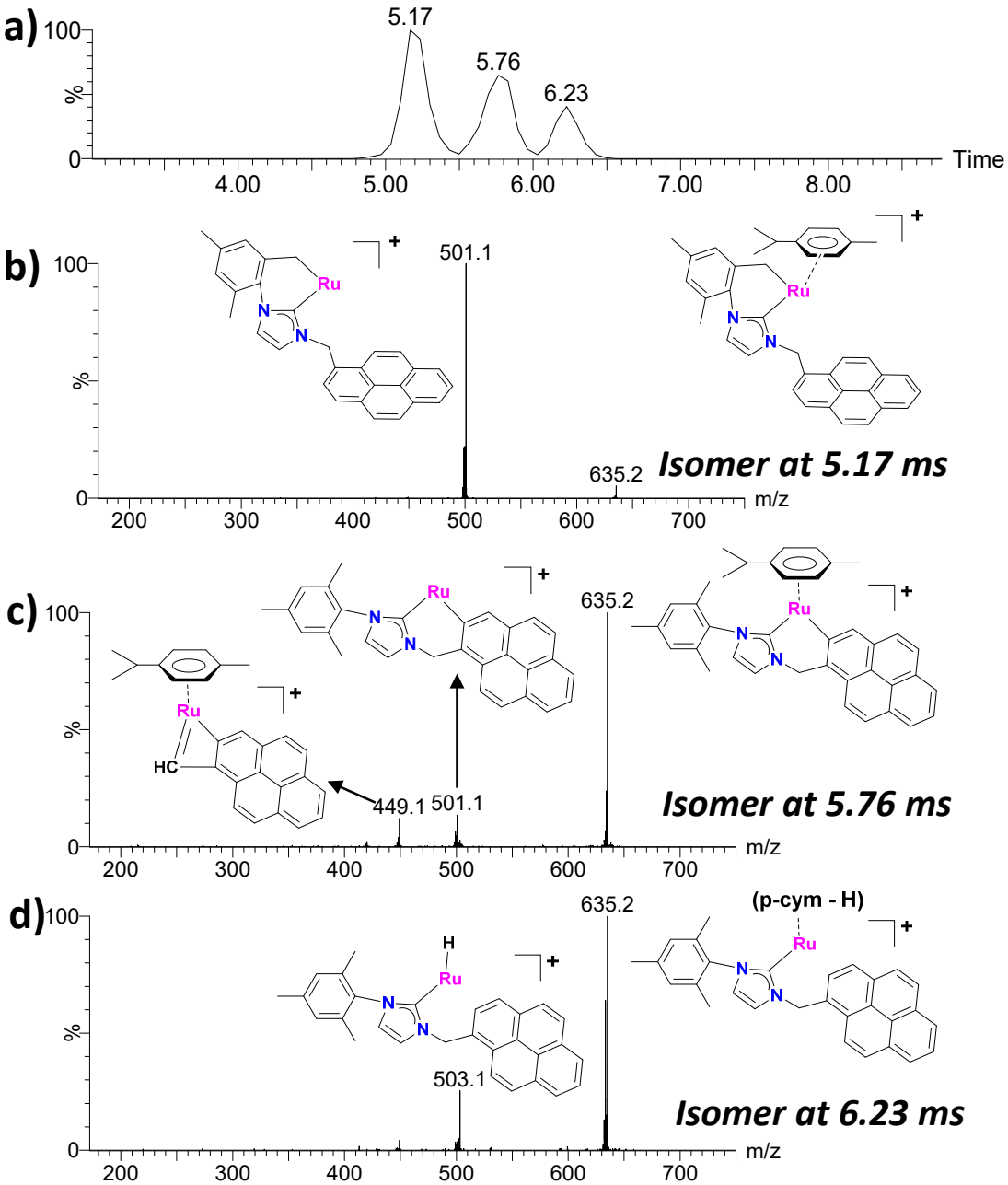

Figure 4. a) ATDs of the product ion at *m/z* 635.1 that is formed upon CID from the precursor $[(NHC^4)(p\text{-cym})RuCl]^+$ ion. Second-generation product ions from the ion mobility-resolved isomers using 25 V and 30 V in the trap and transfer regions, respectively; b) isomer at 5.17 ms; c) isomer at 5.76 ms and d) isomer at 6.23 ms together. Tentative assignment of the isomers is included on the basis of the identity of the second-generation product ions.

Next, we analyzed the effect of C-H bond activation on the topology (size and shape) of the cyclometalated complexes on the basis of their respective Collision Cross Sections (CCS). Hence, only CCS values for the product ions involving cyclometalated species originated by

dehydrogenation from the NHC ligands are considered. From the observed drift times of the precursor and product ions, their corresponding $^{TW}CCS_{N2}$ values ($^{TW}CCS_{N2}$ refers to the determined CCS values using a Travelling Wave Ion Mobility (TWIM) instrument and nitrogen as buffer gas) were estimated by the calibration method.[69,70] Table 1 collects the $^{TW}CCS_{N2}$ values for selected precursor/product cations.

Table 1. Drift times and $^{TW}CCS_{N2}$ calculated values of the complexes under study and their cyclometalated isomers upon CID conditions.

Entry	Precursor / Product ion	$^{TW}CCS_{N2}$[a] (Å^2)
1	$[(NHC^1)PdCl]^+$ / $[(NHC^1 - H)Pd]^+$	212 / 203
2	$[(NHC^1)Cp^*IrCl]^+$ / $[(NHC^1 - H)Cp^*Ir]^+$	253 / 236
3	$[(NHC^2)Cp^*IrCl]^+$ / $[(NHC^2 - H)Cp^*Ir]^+$	217 / 216
4	$[(NHC^2)(p\text{-cym})RuCl]^+$ / $[(NHC^2 - H)(p\text{-cym})Ru]^+$	208 / 218
5	$[(NHC^2)PdBr]^+$ / $[(NHC^2 - H)Pd]^+$	207 / 213
6	$[(NHC^4)(p\text{-cym})RuCl]^+$ / $[(NHC^4 - H)(p\text{-cym})Ru]^{+,c}$	232 / 228$^{C(sp3)-H}$, 243$^{C(sp2)-H}$

[a] Values obtained by calibrating the drift time scale of the TWIM device with standards of known $^{DT}CCS_{N2}$ ($^{DT}CCS_{N2}$ refers to the determined CCS values using a drift tube instrument and nitrogen as buffer gas) cross-sectional data from the literature. [b]Samples were measured by triplicate, and standard deviations were below 0.5 %. [c] $^{TW}CCS_{N2}$ values for the isomers that results from the C(sp3)-H or C(sp2)-H bond activation at the mesityl or pyrene groups are included.

We noticed a significant $^{TW}CCS_{N2}$ increase with the bulkiness of the ligands, as illustrated for the bulkier NHC^1 ligand (1: R = R' = 3,4,5-trimethoxybenzyl) over the NHC^2 ligand (2: R = Me, R' = Pyr) at parity of metal (Ir) and ligand (Cp*) (entries 2 and 3). Likewise, species featuring the NHC^4 ligand (4: R = Mes, R' = Pyr) display larger $^{TW}CCS_{N2}$ values than the NHC^2 (entries 6 and 4) Ru homologues. The $[(NHC^3)(p\text{-cym})RuCl]^+$ complex displayed the lowest $^{TW}CCS_{N2}$ value (165 Å^2) in agreement with the smallest nature of the N-methyl substituted NHC^3 ligand. As far as the cyclometalated product ions is concerned, substantially smaller $^{TW}CCS_{N2}$ values (a 4 % and 7 % $^{TW}CCS_{N2}$ reduction) are evidenced upon cyclometalation of the complexes with the NHC^1 series (entries 1 and 2). This CCS reduction can be intuitively attributed to the elimination of the Cl anion and also to the recoilment of one of the N-bound groups of the NHC^1 ligand upon cyclometalation. The series of cations with the pyrene-tagged NHC^2 ligand displayed the opposite trend. Virtually identical $^{TW}CCS_{N2}$ values (or a slightly increase of 3-5 % $^{TW}CCS_{N2}$) are experienced upon cyclometalation for the NHC^2-containing cations (see entries 3-5). The $[(NHC^4 - H)(p\text{-cym})Ru]^+$ cation indeed corresponds to two isomers that results from the C(sp3)-H or C(sp2)-H bond activation at the mesityl or pyrene groups. Such isomers display smaller (ca. 2 %) and larger (ca. 5 %) $^{TW}CCS_{N2}$ values than their corresponding parent $[(NHC^4)(p\text{-}$

cym)RuCl]$^+$ ion (see entry 6) and are consistent with the previously observed larger $^{TW}CCS_{N2}$ values for the cyclometalated N-bound pyrene groups in the NHC^2 ligand.

Insights on the unique rearrangement suffered by the NHC^2 ligand upon cyclometalation were extracted from DFT calculations of the cations [(NHC^2)(p-cym)RuCl]$^+$ and its corresponding product [(NHC^2 - H)(p-cym)Ru]$^+$ ion. An inspection of the DFT optimized molecular models suggests that the loss of a HCl from the parent [(NHC^2)(p-cym)RuCl]$^+$ has a dramatic effect on conformation of the NHC^2 ligand as well as the pyrene group around the Ru center. The most stable conformation of the precursor [(NHC^2)(p-cym)RuCl]$^+$ resulted the one having the isopropyl group from the p-cymene and the Cl atom located at the opposite side of the pyrene moiety (see figure 5). However, upon cyclometalation, the NHC^2 ring is reoriented around the Ru-p-cymene group accompanied by a turning of the CH_2-pyrene group. As illustrated in figure 5, such rearrangement leaves the pyrene group in a more expanded fashion, which could explain the enhanced $^{TW}CCS_{N2}$ value upon cyclometallation. To validate this hypothesis, the DFT-optimized structures were used as inputs for CCS predictions, and then these were compared with the experimental $^{TW}CCS_{N2}$ data obtained by IM-MS. The CCS values for the [(NHC^2)(p-cym)RuCl]$^+$/[(NHC^2 - H)(p-cym)Ru]$^+$ were calculated using Trajectory Methods (TM) as implemented in the IMoS software.[71] The calculated structures of the model [(NHC^2)(p-cym)RuCl]$^+$ cation and its cyclometalated [(NHC^2 - H)(p-cym)Ru]$^+$ homologue display predicted CCS values of 204 Å^2 and 210 Å^2, respectively that consistently reproduced the experimental $^{TW}CCS_{N2}$ trend (208 Å^2 and 218 Å^2).

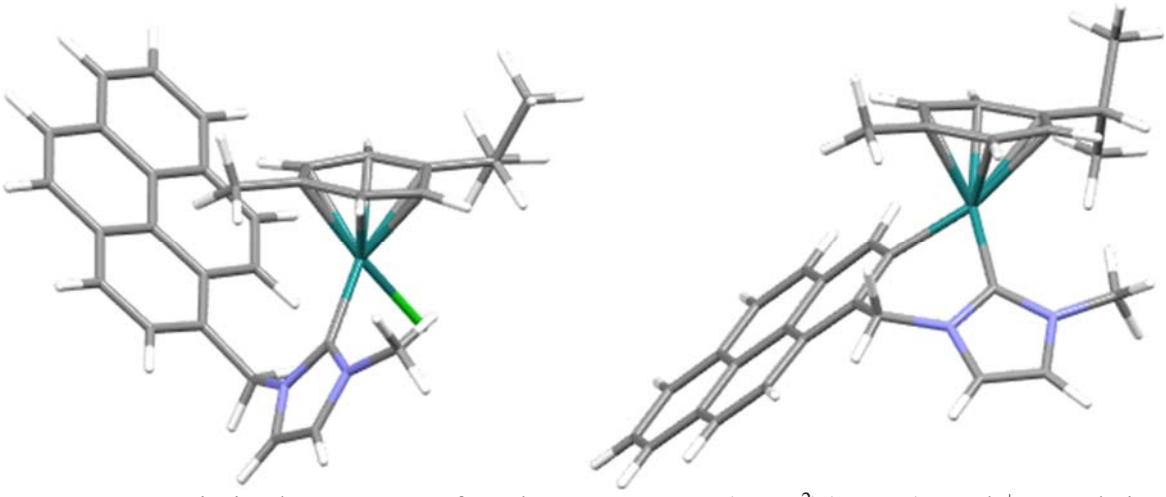

Figure 5. DFT optimized structures for the precursor [(NHC^2)(p-cym)RuCl]$^+$ and its corresponding cyclometalated product ion [(NHC^2 - H)(p-cym)Ru]$^+$ produced upon CID conditions; identical Ru(p-cymene) orientations are shown for clarity.

Conclusions

When studying the mechanism of challenging C-H activations, most reaction pathways often involve highly reactive intermediates, which are key to our understanding, but difficult to study. Therefore, we turned out attention to gas-phase experiments using Mass Spectrometry (MS) methods, which could greatly simplify the study of such processes. The site-selective C-H bond activation of a series of NHC complexes of Pd, Ir and Ru has been investigated in the gas-phase upon CID conditions leading to a series of isomeric cyclometalated product ions. We demonstrate that the use of IM-MS offers a reliable approach to identify site selective C-H bond activation; however, the ability to separate such isomers raises the problem of assigning all the ion-mobility-resolved peaks that are observed. This would require the synthesis of all possible cyclometalated isomers formed upon site-selective C-H bond activation, which is clearly not practical. We turned our attention to the fragmentation of the ion-mobility resolved isomers and we demonstrate that it can be used as an additional structural characterization tool. On the basis of the identity of the second-generation product ions, we are able to assign mobility peaks to specific isomers. This is illustrated for the $[(NHC^4)(p\text{-cym})RuCl]^+$ cation that displays N-bound groups with C(sp2)-H and C(sp3)-H bonds amenable to be metalated upon CID. Together with the well-documented application of ESI-MS and its tandem version for mechanistic studies and the recent developments for "*in-situ*" monitoring and kinetic analysis of the reaction intermediates by MS methods,[72,73] the development of new IM-MS-based approaches have the potential to have an important impact in mechanistic or speciation studies in catalysis. It is reasonable to consider that IM-MS could also be used to identify other site selective C-X bond activation (X = halogen, CN etc..) processes as long as their metalated intermediates formed along the C-X activation paths display distinctive topology.

Experimental Section

Materials and methods. PolyAlanine were purchased from Sigma Aldrich. The NHC complexes used in this study were synthesized as previously reported.[68,74–77]. The synthesis of $[(NHC^4)(p\text{-cym})RuCl_2]$ was carried aout as follows: Silver oxide (73 mg, 0.31 mmol) was added to a solution of 1-mesityl-3- (methylpyrene) imidazolium bromide (150 mg, 0.31 mmol) in CH_3CN in a round bottom flask covered with aluminium foil. The suspension was refluxed for 5 h. Then $[Ru(p\text{-cymene})Cl_2]_2$ (96 mg, 0.15 mmol) was added to the suspension and stirred overnight at reflux temperature. The resulting suspension was filtered through celite and the solvent was removed under reduced pressure. The crude product was purified by column chromatography. The pure compound $[(NHC^4)(p\text{-cym})RuCl_2]$ was eluted with dichloromethane/acetone (9:1) and precipitated in a mixture of dichloromethane/pentane to give a brown solid. Yield: 116 mg (53%).^{1}H NMR (300MHz, $CDCl_3$): δ 8.42(d, $^3J_{H\text{-}H}$ = 9.2 Hz, 1H, CH_{pyr}), 8.22- 8.05 (m, 7H, CH_{pyr}), 7.83 (d, $^3J_{H\text{-}H}$ = 7.9 Hz, 1H, CH_{pyr}), 7.00 (s, 2H, CH_{mes}), 6.90 (d, $^3J_{H\text{-}H}$ = 2.0 Hz, 1H,

CH_{imid}), 6.79 (d, $^3J_{H-H}$ = 1.9 Hz, 1H, CH_{imid}), 6.63 (s, 2H, CH_2), 5.28 (d, $^3J_{H-H}$ = 6.1 Hz, 2H, $CH_{p\text{-cym}}$), 5.11 (d, $^3J_{H-H}$ = 6.1 Hz, 2H, $CH_{p\text{-cym}}$), 2.54 (m, 1H, $CH_{i\text{Pr}}$), 2.36 (s, 3H, $CH_{3,\text{mes}}$), 2.28 (s, 6H, $CH_{3,\text{mes}}$), 1.75 (s, 3H, $CH_{3,p\text{-cym}}$), 1.00 (d, $^3J_{H-H}$ = 7.0 Hz, 6H, $CH_{3,i\text{Pr}}$). $^{13}C\ \{^1H\}$ NMR (75MHz, $CDCl_3$): δ 175.1 ($C_{carbene}$), [139.1, 137.8, 136.7, 134.4, 131.5, 131.2, 130.9, 129.9, 128.8, 128.6, 127.9, 127.4, 126.4, 126.2, 125.7, 125.6, 125.3, 125.1] (C_{pyr}, C_{mes}), 125.0 (CH_{imid}), 124.7 (C_{pyr}), 123.8 (CH_{imid}), 122.8 (CH_{pyr}), [106.1, 94.0] ($C_{p\text{-cym}}$), [87.3, 84.3] ($CH_{p\text{-cym}}$), 54.6 (CH_2), 30.6 ($CH_{i\text{Pr}}$), 22.4 ($CH_{3,i\text{Pr}}$), [21.2, 19.4] ($CH_{3,\text{mes}}$), 18.0 ($CH_{3,p\text{-cym}}$).

ESI Ion Mobility Mass Spectrometry. (ESI-IM-MS). experiments were performed using a SYNAPT XS High Definition Mass Spectrometer (Waters Corporation, Manchester, UK) equipped with an electrospray ionization (ESI) source. A schematic view is given in scheme S1. A capillary voltage was set to 1.5 kV operated in the positive ionization mode and in the resolution mode. Source settings were adjusted to keep intact the complexes of interest. Typical values were cone voltage 20 to 40 V and source offset 4 V; source and desolvation temperatures were set to 110 and 350 ºC, respectively. Cone and desolvation gas flows were 150 and 500 (L/h), respectively. Calibration of the *m/z* axis up to *m/z* 1000 was performed using the routine implemented in intellistart from a mixture of sodium hydroxide and formic acid in 1:9 *v/v* H_2O:isopropanol. The instrument was switched from TOF acquisition to mobility TOF acquisition mode and left for 30 minutes before recording Travelling Wave Ion Mobility (TWIM) mass spectra. The ion mobility separation occurs through the so-called *triwave* device that operates with three regions: trap, ion mobility separation, and transfer with a helium cell located between the trap and ion mobility separation regions. The *m/z* 50-900 range was investigated and ion mobility separation settings were used as follows: the traveling wave height was set to 40 V and wave velocity was set to 650 m/s. The drift gas was nitrogen (N_2) at a flow rate set to 90 mL/min. The helium cell gas flow was 180.00 mL/min. IMS DC values were as follow: Entrance 20; Helium cell DC 50; Helium exit -20; Bias 3; Exit 0. Trap DC bias was 45 V; entrance, 3; Exit 0. The TWIM-MS data were processed using Masslynx 4.2 (SCN 982). Ion mobility spectra of the species of interest were extracted using a 0.15 Da mass window and were converted from waters.raw to .txt files. Gaussian fitting of the IM data was applied to improve the precision of the drift time measurements. The reported drift times values were obtained by Gaussian peak fitting using origin 6.0 (Microcal) rendering good correlation in all cases. In those cases where partial overlapping of the ATD profiles was observed, deconvolution to several gaussian functions was performed. Each sample was recorded by triplicate on the same day and the deviation in the drift time values was less than 0.5 %.

Acetonitrile sample solutions (ca. 10^{-6} M) of the NHC complex of interest were investigated by ESI-MS and ESI-IM-MS. Simulated isotopic patterns were checked for each identified ion and in all cases, they exactly matched the experimental ones, thereby indicating

that ionization of these compounds took place exclusively via the loss of a chloride ligand. ESI Ion mobility (IM) mass spectra were virtually identical to those obtained by single-stage ESI-MS in the absence of mobility separation.

For collision induced dissociation (CID) experiments, the cation of interest was mass-selected with the first quadrupole using an isolation width of 1 Da, interacted with argon in the trap region (prior to the Ion mobility separation) by increasing the applied voltage in the trap (Utrap) and monitoring the ATD characteristics of the product ions while analyzing the ionic fragments with the TOF analyzer. In this particular case, the mass selection of the monoisotopic peak, even though it displays much lower ion counts, was advantageous to clearly differentiate losses of HCl ($H^{35}Cl$ Δm 36) that occurs simultaneously with losses of nH_2 (Δm 2 and 4). Additional experiments were performed in the transfer cell (behind the ion mobility section) section by increasing the applied voltage in the transfer (Utransfer) aimed to prove the additional fragmentation of the previously ion mobility-resolved product ion. When the CID experiment is conducted in transfer section, the generated second-generation product ions will have same drift time as their parent ion in ion mobility mode. The collision energy in the trap region (Utrap) was systematically stepped in the Utrap = 1–30 V range (5 V increments) where the dehydrohalogenation fragmentation step (Δm 36) was dominant. At higher collision energies, complex fragmentation of the NHC backbone and p-cymene or Cp* ligand was observed.

Breakdown profile graphics represents the relative abundance of the precursor and product ions as the collision energy is increased. For these representations, the relative abundance of the precursor ion was calculated as Ip/(Ip+Σ Ifrag), where Ip is the peak intensity of the precursor ion, and Σ Ifrag is the sum of the peak intensities corresponding to all fragments, in most cases the product ion that results from losses of Δm 36. In some cases, several isomers contribute to the ion population of this ion and the branching ratio of each one was extracted from the areas of their mobility peaks from the ATD profiles according to the Russell procedure.[78] Their relative abundances from CID experiments were determined from mass spectra averaged over 120 scans. There was little variation (max. 3%) in the relative product ion abundances from three consecutive CID mass spectra. The collision energy was increased every 5 V in the 1-30 V range and typically 7 CE points were considered to yield a clear picture of the distinctive propensity to eliminate HCl from the Cp*(or p-cym) or the NHC ligand.

CCS Calibration. Drift times were converted into CCS following the CCS calibration protocol reported by Ruotolo.[69] Calibration of the IM device for determining collision cross-sectional areas from drift time measurements was performed using a mixture of polyalanine reference ions covering the transit time of the investigated ions.[70] Their $^{DT}CCS_{N2}$ values were taken from the literature (polyAlanine[79]). As the TWIMS device is operated with N_2 buffer gas, the obtained

^{TW}CCS values will be noted $^{TW}CCS_{N2}$. Drift times (t_D) were subjected to correction for mass-dependent and mass-independent flight times according to $t_D' = t_D - C * \frac{\sqrt{m/z}}{1000} - 0{,}9$ (C = 1.5 and the term 0.9 ms is the mass-independent time to account for the time of transit of one wave in the IM and the transfer region). The literature CCS values were converted to CCS′ according to $CCS' = \frac{CCS\sqrt{\mu}}{z}$ where μ and z stands for the reduced mass of the collision partners and the charge state, respectively. The calibration curve is represented as CCS′ as a function of t_D' using a power law,[80] $CCS' = A \times (t_D')^B$. Constants A and B were subsequently derived from the calibration plot and used to calculate cross-sectional areas ($^{TW}CCS_{N2}$) of unknown species from corrected drift time measurements extracted for specific *m/z* values from the data.

DFT calculations

Geometry optimizations, single-point calculations and frequency calculations were performed using Gaussian 09 suite of programs with the PBE1PBE functional and the LanL2DZ basis for Ru and 6-31G(d) for (C H N O).[81] Frequency calculations were performed on optimized geometries to ensure true minima.

Calculate CCS with TM methods. For Trajectory Methods (TM) calculations, IMoS 1.10 was used.[71] Atomic coordinates were exported as .xyz files from minimized energy models in pdb format. For TM methods, the potentials employed are standard TM Lenard-Jones methods using a 4-6-12 potential. The number of rotations was 3 with 300000 gas molecules per rotations.

Acknowledgments

Thanks to PID2021-126071OB-C22 and PID2021-122900NB-I00 financed by MICIN/AEI/10.13039/501100011033/ FEDER "Una manera de hacer Europa". Generalitat Valenciana (PROMETEU/2020/028) and Universitat Jaume I (UJI-B2018-23). L. I-I. thanks MIU (FPU20/04385) for a grant. The authors thank 'Servei Central d'Instrumentació Científica (SCIC) de la Universitat Jaume I'. G. G.-B gratefully acknowledges (RYC2019-026693-I/AEI/10.13039/501100011033) "El Fondo Social Europeo invierte en tu futuro' and to the Gobierno de Aragón/FEDER, UE (GA/FEDER, Reactividad y catálisis en química inorgánica, Group E50_20D). The authors would like to acknowledge the use of 'Servicio General de Apoyo a la Investigación-SAI, Universidad de Zaragoza'.

References

(1) van der Boom, M. E.; Milstein, D. Cyclometalated Phosphine-Based Pincer Complexes: Mechanistic Insight in Catalysis, Coordination, and Bond Activation. *Chem. Rev.* **2003**, *103* (5), 1759–1792.

(2) Albrecht, M. Cyclometalation Using D-Block Transition Metals: Fundamental Aspects and Recent Trends. *Chem. Rev.* **2010**, *110* (2), 576–623.

(3) Han, Y. F.; Jin, G. X. Cyclometalated [Cp*M(C^X)] (M = Ir, Rh; X = N, C, O, P) Complexes. *Chem. Soc. Rev.* **2014**, *43* (8), 2799–2823.

(4) Dalton, T.; Faber, T.; Glorius, F. C-H Activation: Toward Sustainability and Applications *ACS Cent. Sci.* **2021**, *7* (2), 245–261.

(5) Zhao, Q.; Meng, G.; Nolan, S. P.; Szostak, M. N-Heterocyclic Carbene Complexes in C-H Activation Reactions. *Chem. Rev.* **2020**, *120* (4), 1981–2048.

(6) van Vuuren, E.; Malan, F. P.; Landman, M. Multidentate NHC Complexes of Group IX Metals Featuring Carbon-Based Tethers: Synthesis and Applications. *Coord. Chem. Rev.* **2021**, *430*, 213731.

(7) Tiwari, C. S.; Illam, P. M.; Donthireddy, S. N. R.; Rit, A. Recent Advances in the Syntheses and Catalytic Applications of Homonuclear Ru-, Rh-, and Ir-Complexes of CNHC^C Cyclometalated Ligands. *Chem. - A Eur. J.* **2021**, *27* (67), 16581–16600.

(8) Burling, S.; Paine, B. M.; Nama, D.; Brown, V. S.; Mahon, M. F.; Prior, T. J.; Pregosin, P. S.; Whittlesey, M. K.; Williams, J. M. J. C-H Activation Reactions of Ruthenium N-Heterocyclic Carbene Complexes: Application in a Catalytic Tandem Reaction Involving CC Bond Formation from Alcohols. *J. Am. Chem. Soc.* **2007**, *129* (7), 1987–1995.

(9) Ritleng, V.; de Vries, J. G. Ruthenacycles and Iridacycles as Transfer Hydrogenation Catalysts. *Molecules* **2021**, *26* (13).

(10) Nakajima, I.; Shimizu, M.; Okuda, Y.; Akiyama, R.; Tadano, R.; Nagaoka, M.; Uemura, N.; Yoshida, Y.; Mino, T.; Shinozaki, H.; Yamamoto, T. Synthesis and Catalysis of NHC Coordinated Cyclometalated Palladium(II) Complexes with Bridging Hydroxide Ligands. *Adv. Synth. & Catal.* **2022**, *364* (10), 1763–1768.

(11) Schroeter, F.; Soellner, J.; Strassner, T. Cyclometalated Palladium NHC Complexes Bearing PEG Chains for Suzuki–Miyaura Cross-Coupling in Water. *Organometallics* **2018**, *37* (22), 4267–4275.

(12) Paul, D.; Beiring, B.; Plois, M.; Ortega, N.; Kock, S.; Schlüns, D.; Neugebauer, J.; Wolf, R.; Glorius, F. Cyclometalated Ruthenium-NHC Precatalyst for the Asymmetric Hydrogenation of (Hetero)Arenes and Its Activation Pathway. *Organometallics* **2016**, *35* (20), 3641–3646.

(13) Janssen-Müller, D.; Schlepphorst, C.; Glorius, F. Privileged Chiral N-Heterocyclic Carbene Ligands for Asymmetric Transition-Metal Catalysis. *Chem. Soc. Rev.* **2017**, *46* (16), 4845–4854.

(14) Bauri, S.; Mallik, A.; Rit, A. Naphthyl-Derived Orthometalated RUII-NHC Complexes: Effect of the NHC Donors and/or Substitution Pattern on Their Synthesis and Catalytic Activity.*Organometallics* **2020**, *39* (18), 3362–3374.

(15) Xie, X.; Huynh, H. V. Cyclometallated Ruthenium(Ii) Complexes with Ditopic Thienyl–NHC Ligands: Syntheses and Alkyne Annulations. *Org. Chem. Front.* **2015**, *2* (12), 1598–1603.

(16) Ma, C.; Ai, C.; Li, Z.; Li, B.; Song, H.; Xu, S.; Wang, B. Synthesis and Alkyne Insertion Reactions of NHC-Based Cyclometalated Ruthenium(II) Complexes. *Organometallics* **2014**, *33* (19), 5164–5172.

(17) Dutta, C.; Choudhury, J. C-H Activation-Annulation on the N-Heterocyclic Carbene Platform. *RSC Adv.* **2018**, *8* (49), 27881–27891.

(18) Liu, H. J.; Raynaud, C.; Eisenstein, O.; Tilley, T. D. Cyclometalated N-Heterocyclic

Carbene Complexes of Ruthenium for Access to Electron-Rich Silylene Complexes That Bind the Lewis Acids CuOTf and AgOTf. *J. Am. Chem. Soc.* **2014**, *136* (32), 11473–11482.

(19) Liu, H. J.; Guihaumé, J.; Davin, T.; Raynaud, C.; Eisenstein, O.; Tilley, T. D. 1,2-Hydrogen Migration To a Saturated Ruthenium Complex Via Reversal of Electronic Properties for Tin in a Stannylene-To-Metallostannylene Conversion. *J. Am. Chem. Soc.* **2014**, *136* (40), 13991–13994.

(20) Tamosiunaite, N.; Logie, L. C.; Neale, S. E.; Singh, K.; Davies, D. L.; Macgregor, S. A. Experimental and Computational Studies on the Acetate-Assisted C–H Activation of N-Aryl Imidazolium Salts at Rhodium and Iridium: A Chloride Additive Changes the Selectivity of C–H Activation. *J. Org. Chem.* **2022**, *87* (2), 1445–1456.

(21) Taghizadeh Ghoochany, L.; Kerner, C.; Farsadpour, S.; Menges, F.; Sun, Y.; Niedner-Schatteburg, G.; Thiel, W. R. C-H Activation at a Ruthenium(II) Complex - The Key Step for a Base-Free Catalytic Transfer Hydrogenation? *Eur. J. Inorg. Chem.* **2013**, No. 24, 4305–4317.

(22) Fizia, A.; Gaffga, M.; Lang, J.; Sun, Y.; Niedner-Schatteburg, G.; Thiel, W. R. Cyclopalladation in the Periphery of a NHC Ligand as the Crucial Step in the Synthesis of Highly Active Suzuki–Miyaura Cross-Coupling Catalysts. *Chem. – A Eur. J.* **2017**, *23* (58), 14563–14575.

(23) Semwal, S.; Ghorai, D.; Choudhury, J. Wingtip-Dictated Cyclometalation of N-Heterocyclic Carbene Ligand Framework and Its Implication toward Tunable Catalytic Activity. *Organometallics* **2014**, *33* (24), 7118–7124.

(24) Balamurugan, G.; Ramesh, R.; Malecki, J. G. Cyclometalated Ru(II)-NHC Complexes as Effective Catalysts for Transfer Hydrogenation: Influence of Wingtip Group on Catalytic Outcome. *ChemistrySelect* **2017**, *2* (32), 10603–10608.

(25) Choi, G.; Tsurugi, H.; Mashima, K. Hemilabile N-Xylyl-N′-Methylperimidine Carbene Iridium Complexes as Catalysts for C–H Activation and Dehydrogenative Silylation: Dual Role of N-Xylyl Moiety for Ortho-C–H Bond Activation and Reductive Bond Cleavage. *J. Am. Chem. Soc.* **2013**, *135* (35), 13149–13161.

(26) Burling, S.; Mahon, M. F.; Paine, B. M.; Whittlesey, M. K.; Williams, J. M. J. Reversible Intramolecular Alkyl C-H Bond Activation, Alcohol Dehydrogenation, and Trans-Cis Dihydride Isomerization in Ruthenium N-Heterocyclic Carbene Complexes. *Organometallics* **2004**, *23* (20), 4537–4539.

(27) Bauri, S.; Donthireddy, S. N. R.; Illam, P. M.; Rit, A. Effect of Ancillary Ligand in Cyclometalated Ru(II)-NHC-Catalyzed Transfer Hydrogenation of Unsaturated Compounds. *Inorg. Chem.* **2018**, *57* (23), 14582–14593.

(28) Liu, H. J.; Ziegler, M. S.; Tilley, T. D. Synthesis, Structures, and Reactivity Studies of Cyclometalated N-Heterocyclic Carbene Complexes of Ruthenium. *Dalton Trans.* **2018**, *47* (35), 12138–12146.

(29) Młodzikowska-Pieńko, K.; Trzaskowski, B. Rate-Limiting Steps in the Intramolecular C–H Activation of Ruthenium N-Heterocyclic Carbene Complexes. *J. Phys. Chem. A* **2020**, *124* (18), 3609–3617.

(30) Zhang, C.; Zhao, Y.; Li, B.; Song, H.; Xu, S.; Wang, B. The Intramolecular Sp2 and Sp3 C-H Bond Activation of (p-Cymene)Ruthenium(Ii) N-Heterocyclic Carbene Complexes. *Dalton Trans.* **2009**, 26, 5182–5189.

(31) Liang, Q.; Song, D. Reactivity of Fe and Ru Complexes of Picolyl-Substituted N-Heterocyclic Carbene Ligand: Diverse Coordination Modes and Small Molecule Binding. *Inorg. Chem.* **2017**, *56* (19), 11956–11970.

(32) Fehér, P. P.; Horváth, H.; Joó, F.; Purgel, M. DFT Study on the Mechanism of Hydrogen Storage Based on the Formate-Bicarbonate Equilibrium Catalyzed by an Ir-NHC Complex: An Elusive Intramolecular C–H Activation. *Inorg. Chem.* **2018**, *57* (10), 5903–5914.

(33) Wada, Y.; Takehara, T.; Suzuki, T.; Aoki, S.; Hibi, T.; Sako, M.; Tsujino, H.; Tsutsumi, Y.; Arisawa, M. Carbon-Carbon Bond Formation between N-Heterocyclic Carbene Ligand on Ruthenium Carbene Catalysts and 1,4-Naphthoquinone via Intramolecular Carbon(Sp3)-Hydrogen Bond Activation. *Organometallics* **2021**, *40* (16), 2901–2908.

(34) Roithová, J.; Schröder, D. Selective Activation of Alkanes by Gas-Phase Metal Ions. *Chem. Rev.* **2010**, *110* (2), 1170–1211.

(35) Mehara, J.; Roithová, J. Identifying Reactive Intermediates by Mass Spectrometry. *Chem. Sci.* **2020**, *11* (44), 11960–11972.

(36) Chen, P. Electrospray Ionization Tandem Mass Spectrometry in High-Throughput Screening of Homogeneous Catalysts. *Angew. Chemie Int. Ed.* **2003**, *42* (25), 2832–2847.

(37) Schröder, D. Applications of Electrospray Ionization Mass Spectrometry in Mechanistic Studies and Catalysis Research. *Acc. Chem. Res.* **2012**, *45* (9), 1521–1532.

(38) Iacobucci, C.; Reale, S.; De Angelis, F. Elusive Reaction Intermediates in Solution Explored by ESI-MS: Reverse Periscope for Mechanistic Investigations. *Angew. Chemie Int. Ed.* **2016**, *55* (9), 2980–2993.

(39) Santos, L. S. Online Mechanistic Investigations of Catalyzed Reactions by Electrospray Ionization Mass Spectrometry: A Tool to Intercept Transient Species in Solution. *Eur. J. Org. Chem.* **2008**, *2008* (2), 235–253.

(40) Yunker, L. P. E.; Stoddard, R. L.; McIndoe, J. S. Practical Approaches to the ESI-MS Analysis of Catalytic Reactions. *J. Mass Spectrom.* **2014**, *49* (1), 1–8.

(41) Vikse, K. L.; Ahmadi, Z.; Scott McIndoe, J. The Application of Electrospray Ionization Mass Spectrometry to Homogeneous Catalysis. *Coord. Chem. Rev.* **2014**, *279*, 96–114.

(42) Cheng, G. J.; Zhong, X. M.; Wu, Y. D.; Zhang, X. Mechanistic Understanding of Catalysis by Combining Mass Spectrometry and Computation. *Chem. Commun.* **2019**, *55* (85), 12749–12764.

(43) Chen, Q.; Liu, Q.; Xiao, J.; Leng, X.; Deng, L. Catalytic Method for the Synthesis of Deuterium-Labeled N-Heterocyclic Carbenes Enabled by a Coordinatively Unsaturated Ruthenium N-Heterocyclic Carbene Catalyst. *J. Am. Chem. Soc.* **2021**, *143* (47), 19956–19965.

(44) Lanucara, F.; Holman, S. W.; Gray, C. J.; Eyers, C. E. The Power of Ion Mobility-Mass Spectrometry for Structural Characterization and the Study of Conformational Dynamics. *Nat. Chem.* **2014**, *6* (4), 281–294.

(45) Kalenius, E.; Groessl, M.; Rissanen, K. Ion Mobility–Mass Spectrometry of Supramolecular Complexes and Assemblies. *Nat. Rev. Chem.* **2019**, *3* (1), 4–14.

(46) Tsybizova, A.; Rulíšek, L.; Schröder, D.; Rokob, T. A. Coordination and Bond Activation in Complexes of Regioisomeric Phenylpyridines with the Nickel(II) Chloride Cation in the Gas Phase. *J. Phys. Chem. A* **2013**, *117* (6), 1171–1180.

(47) Ducháčková, L.; Roithová, J.; Milko, P.; Zabka, J.; Tsierkezos, N.; Schroder, D. Comparative Study of Mono-and Dinuclear Complexes of Late 3d-Metal Chlorides with N,N-Dimethylformamide in the Gas Phase. *Inorg. Chem.* **2011**, *50* (3), 771–782.

(48) Czerwinska, I.; Far, J.; Kune, C.; Larriba-Andaluz, C.; Delaude, L.; De Pauw, E. Structural Analysis of Ruthenium-Arene Complexes Using Ion Mobility Mass Spectrometry, Collision-Induced Dissociation, and DFT. *Dalton Trans.* **2016**, *45* (15), 6361–6370.

(49) Williams, J. P.; Bugarcic, T.; Habtemariam, A.; Giles, K.; Campuzano, I.; Rodger, P. M.; Sadler, P. J. Isomer Separation and Gas-Phase Configurations of Organoruthenium Anticancer Complexes: Ion Mobility Mass Spectrometry and Modeling. *J. Am. Soc. Mass Spectrom.* **2009**, *20* (6), 1119–1122.

(50) Williams, J. P.; Lough, J. A.; Campuzano, I.; Richardson, K.; Sadler, P. J. Use of Ion Mobility Mass Spectrometry and a Collision Cross-Section Algorithm to Study an Organometallic Ruthenium Anticancer Complex and Its Adducts with a DNA Oligonucleotide. *Rapid Commun. Mass Spectrom.* **2009**, *23* (22), 3563–3569.

(51) Fiedler, T.; Chen, L.; Wagner, N. D.; Russell, D. H.; Gladysz, J. A. Gas and Liquid Phase Diffusivities of Isomeric Metal Complexes Derived from Multifold Ring-Closing Metatheses: Ion Mobility Mass Spectrometry Trumps DOSY NMR. *Organometallics* **2016**, *35* (12), 2071–2075.

(52) Cheng, G. J.; Chen, P.; Sun, T. Y.; Zhang, X.; Yu, J. Q.; Wu, Y. D. A Combined IM-MS/DFT Study on [Pd(MPAA)]-Catalyzed Enantioselective C-H Activation: Relay of Chirality through a Rigid Framework. *Chem. - A Eur. J.* **2015**, *21* (31), 11180–11188.

(53) Song, L. J.; Wang, T.; Zhang, X.; Chung, L. W.; Wu, Y. D. A Combined DFT/IM-MS Study on the Reaction Mechanism of Cationic Ru(II)-Catalyzed Hydroboration of Alkynes. *ACS Catal.* **2017**, *7* (2), 1361–1368.

(54) Shaffer, C. J.; Schröder, D.; Gütz, C.; Lützen, A. Intramolecular C-H Bond Activation through a Flexible Ester Linkage. *Angew. Chemie - Int. Ed.* **2012**, *51* (32), 8097–8100.

(55) Greisch, J.-F.; Weis, P.; Brendle, K.; Kappes, M. M.; Haler, J. R. N.; Far, J.; De Pauw, E.; Albers, C.; Bay, S.; Wurm, T.; Rudolph, M.; Schulmeister, J.; Hashmi, A. S. K. Detection of Intermediates in Dual Gold Catalysis Using High-Resolution Ion Mobility Mass Spectrometry. *Organometallics* **2018**, *37* (9), 1493–1500.

(56) Hilgers, R.; Yong Teng, S.; Briš, A.; Pereverzev, A. Y.; White, P.; Jansen, J. J.; Roithová, J. Monitoring Reaction Intermediates to Predict Enantioselectivity Using Mass Spectrometry. *Angew. Chem. Int. Ed.* **2022**, doi.org/10.1002/anie.202205720.

(57) Henderson, W.; Evans, C. Electrospray Mass Spectrometric Analysis of Transition-Metal Halide Complexes. *Inorg. Chim. Acta* 1999, *294* (2), 183–192.

(58) Nasielski, J.; Hadei, N.; Achonduh, G.; Kantchev, E. A. B.; O'Brien, C. J.; Lough, A.; Organ, M. G. tructure–Activity Relationship Analysis of Pd–PEPPSI Complexes in Cross-Couplings: A Close Inspection of the Catalytic Cycle and the Precatalyst Activation Model *Chem. – A Eur. J.* 2010, *16* (35), 10844–10853.

(59) Briš, A.; Turel, I.; Roithová, J. C–H Bond Activation by a Ruthenium(II) β-Diketonate Complex: A Mechanistic Study. *European J. Org. Chem.* **2018**, *2018* (44), 6107–6113.

(60) Menges, F. S.; Lang, J.; Nosenko, Y.; Kerner, C.; Gaffga, M.; Ghoochany, L. T.; Thiel, W. R.; Riehn, C.; Niedner-Schatteburg, G. Exploring the Gas-Phase Activation and Reactivity of a Ruthenium Transfer Hydrogenation Catalyst by Experiment and Theory in Concert. *J. Phys. Chem. A* **2017**, *121* (23), 4422–4434.

(61) Kerner, C.; Lang, J.; Gaffga, M.; Menges, F. S.; Sun, Y.; Niedner-Schatteburg, G.; Thiel, W. R. Mechanistic Studies on Ruthenium(II)-Catalyzed Base-Free Transfer Hydrogenation Triggered by Roll-Over Cyclometalation.*Chempluschem* **2017**, *82* (2), 212–224.

(62) Butschke, B.; Schlangen, M.; Schröder, D.; Schwarz, H. Roll-over" Cyclometalation of 2,2′-Bipyridine Platinum(II) Complexes in the Gas Phase: A Combined Experimental and Computational Study *Chem. - A Eur. J.* **2008**, *14* (35), 11050–11060.

(63) Butschke, B.; Schwarz, H. Mechanistic Study on the Gas-Phase Generation of "Rollover"-Cyclometalated [M(Bipy − H)]+ (M = Ni, Pd, Pt). *Organometallics* **2010**, *29* (22), 6002–6011.

(64) Butschke, B.; Schwarz, H. rollover Cyclometalation - Early History, Recent Developments, Mechanistic Insights and Application *Chem. Sci.* **2012**, *3* (2), 308–326.

(65) Leist, M.; Kerner, C.; Ghoochany, L. T.; Farsadpour, S.; Fizia, A.; Neu, J. P.; Schön, F.; Sun, Y.; Oelkers, B.; Lang, J.; Menges, F.; Niedner-Schatteburg, G.; Salih, K. S. M.; Thiel, W. R. Roll-over Cyclometalation: A Versatile Tool to Enhance the Catalytic Activity of Transition Metal Complexes. *J. Organomet. Chem.* **2018**, *863*, 30–43.

(66) Becker, Y.; Huber, M.; Becker, S.; Sun, Y.; Niedner-Schatteburg, G.; Thiel, W. R. Gas-Phase Study on the Cyclometallation of a Series of Cp*Ir(III) Complexes Bearing Bidentate Pyrimidine Ligands. *J. Organomet. Chem.* **2021**, *954–955*, 122063.

(67) Kerner, C.; Neu, J. P.; Gaffga, M.; Lang, J.; Oelkers, B.; Sun, Y.; Niedner-Schatteburg, G.; Thiel, W. R. Gas-phase reactivity of Cp* group IX metal complexes bearing aromatic N, N′-chelating ligands. *New J. Chem.* **2017**, *41* (15), 6995–7006.

(68) Ventura-Espinosa, D.; Sabater, S.; Carretero-Cerdán, A.; Baya, M.; Mata, J. A. High Production of Hydrogen on Demand from Silanes Catalyzed by Iridium Complexes as a Versatile Hydrogen Storage System. *ACS Catal.* **2018**, *8* (3), 2558–2566.

(69) Ruotolo, B. T.; Benesch, J. L. P.; Sandercock, A. M.; Hyung, S.-J.; Robinson, C. V. Ion Mobility–Mass Spectrometry Analysis of Large Protein Complexes. *Nat. Protoc.* **2008**, *3* (7), 1139–1152.

(70) Gabelica, V.; Shvartsburg, A. A.; Afonso, C.; Barran, P.; Benesch, J. L. P.; Bleiholder, C.; Bowers, M. T.; Bilbao, A.; Bush, M. F.; Campbell, J. L.; Campuzano, I. D. G.; Causon, T.; Clowers, B. H.; Creaser, C. S.; De Pauw, E.; Far, J.; Fernandez-Lima, F.; Fjeldsted, J. C.; Giles, K.; Groessl, M.; Hogan Jr, C. J.; Hann, S.; Kim, H. I.; Kurulugama, R. T.; May, J. C.; McLean, J. A.; Pagel, K.; Richardson, K.; Ridgeway, M. E.; Rosu, F.; Sobott, F.; Thalassinos, K.; Valentine, S. J.; Wyttenbach, T. Recommendations for Reporting Ion Mobility Mass Spectrometry Measurements. *Mass Spectrom. Rev.* **2019**, *38* (3), 291–320.

(71) Coots, J.; Gandhi, V.; Onakoya, T.; Chen, X.; Larriba-Andaluz, C. A Parallelized Tool to Calculate the Electrical Mobility of Charged Aerosol Nanoparticles and Ions in the Gas Phase. *J. Aerosol Sci.* **2020**, *147*, 105570.

(72) Thomas, G. T.; Donnecke, S.; Chagunda, I. C.; McIndoe, J. S. Pressurized Sample Infusion. *Chemistry–Methods* **2022**, doi.org/https://doi.org/10.1002/cmtd.202100068.

(73) Tripodi, G. L.; Derks, M. T. G. M.; Rutjes, F. P. J. T.; Roithová, J. Tracking Reaction Pathways by a Modular Flow Reactor Coupled to Electrospray Ionization Mass Spectrometry. *Chemistry–Methods* **2021**, *1* (10), 430–437.

(74) Mollar-Cuni, A.; Ventura-Espinosa, D.; Martín, S.; Mayoral, Á.; Borja, P.; Mata, J. A. Stabilization of Nanoparticles Produced by Hydrogenation of Palladium–N-Heterocyclic

Carbene Complexes on the Surface of Graphene and Implications in Catalysis. *ACS Omega* **2018**, *3* (11), 15217–15228.

(75) Ventura-Espinosa, D.; Carretero-Cerdán, A.; Baya, M.; García, H.; Mata, J. A. Catalytic Dehydrogenative Coupling of Hydrosilanes with Alcohols for the Production of Hydrogen On-Demand: Application of a Silane/Alcohol Pair as a Liquid Organic Hydrogen Carrier. *Chem. – A Eur. J.* **2017**, *23* (45), 10815–10821.

(76) Ventura-Espinosa, D.; Marzá-Beltrán, A.; Mata, J. A. Catalytic Hydrogen Production by Ruthenium Complexes from the Conversion of Primary Amines to Nitriles: Potential Application as a Liquid Organic Hydrogen Carrier. *Chem. – A Eur. J.* **2016**, *22* (49), 17758–17766.

(77) Sabater, S.; Mata, J. A.; Peris, E. Catalyst Enhancement and Recyclability by Immobilization of Metal Complexes onto Graphene Surface by Noncovalent Interactions. *ACS Catal.* **2014**, *4* (6), 2038–2047.

(78) Mallis, C. S.; Saha, M. L.; Stang, P. J.; Russell, D. H. Topological Characterization of Coordination-Driven Self-Assembly Complexes: Applications of Ion Mobility-Mass Spectrometry. *J. Am. Soc. Mass Spectrom.* **2019**, *30* (9), 1654–1662.

(79) Bush, M. F.; Campuzano, I. D. G.; Robinson, C. V. Ion Mobility Mass Spectrometry of Peptide Ions: Effects of Drift Gas and Calibration Strategies. *Anal. Chem.* **2012**, *84* (16), 7124–7130.

(80) Williams, J. P.; Scrivens, J. H. Coupling Desorption Electrospray Ionisation and Neutral Desorption/Extractive Electrospray Ionisation with a Travelling-Wave Based Ion Mobility Mass Spectrometer for the Analysis of Drugs. *Rapid Commun. Mass Spectrom.* **2008**, *22* (2), 187–196.

(81) Frisch, M. J.; Trucks, G. W.; Schlegel, H. B.; Scuseria, G. E.; Robb, M. A. . C.; J. R.; Scalmani, G.; Barone, V.; Mennucci, B.; Petersson, G. A.; Nakatsuji, H. . C.; M.; Li, X.; Hratchian, H. P.; Izmaylov, A. F.; Bloino, J.; Zheng, G.; Sonnenberg, J. L. .; Hada, M.; Ehara, M.; Toyota, K.; Fukuda, R.; Hasegawa, J.; Ishida, M.; Nakajima, T. .; Honda, Y.; Kitao, O.; Nakai, H.; Vreven, T.; Montgomery, J. A.; Peralta, J. E. . O.; F.; Bearpark, M.; Heyd, J. J.; Brothers, E.; Kudin, K. N.; Staroverov, V. N. . K.; R.; Normand, J.; Raghavachari, K.; Rendell, A.; Burant, J. C.; Iyengar, S. S.; Tomasi, J. .; Cossi, M.; Rega, N.; Millam, J. M.; Klene, M.; Knox, J. E.; Cross, J. B.; Bakken, V. .; Adamo, C.; Jaramillo, J.; Gomperts, R.; Stratmann, R. E.; Yazyev, O.; Austin, A. J. .; Cammi, R.; Pomelli, C.; Ochterski, J. W.; Martin, R. L.; Morokuma, K.; Zakrzewski, V.; G.; Voth, G. A.; Salvador, P.; Dannenberg, J. J.; Dapprich, S.; Daniels, A. D. . F.; Foresman, J. B.; Ortiz, J. V; Cioslowski, J.; Fox, D. J. Gaussian 09, Revision B.01. *Gaussian 09, Revision B.01, Gaussian, Inc., Wallingford CT*. 2010.

For Table of Contents Use Only

Introducing Ion Mobility Mass Spectrometry to Identify Site-Selective C-H Bond Activation in N-Heterocyclic Carbene Metal Complexes

Andrés Mollar-Cuni,[a] Laura Ibáñez-Ibáñez,[a] Gregorio Guisado-Barrios[b] , Jose A. Mata[a] and Cristian Vicent*[c]

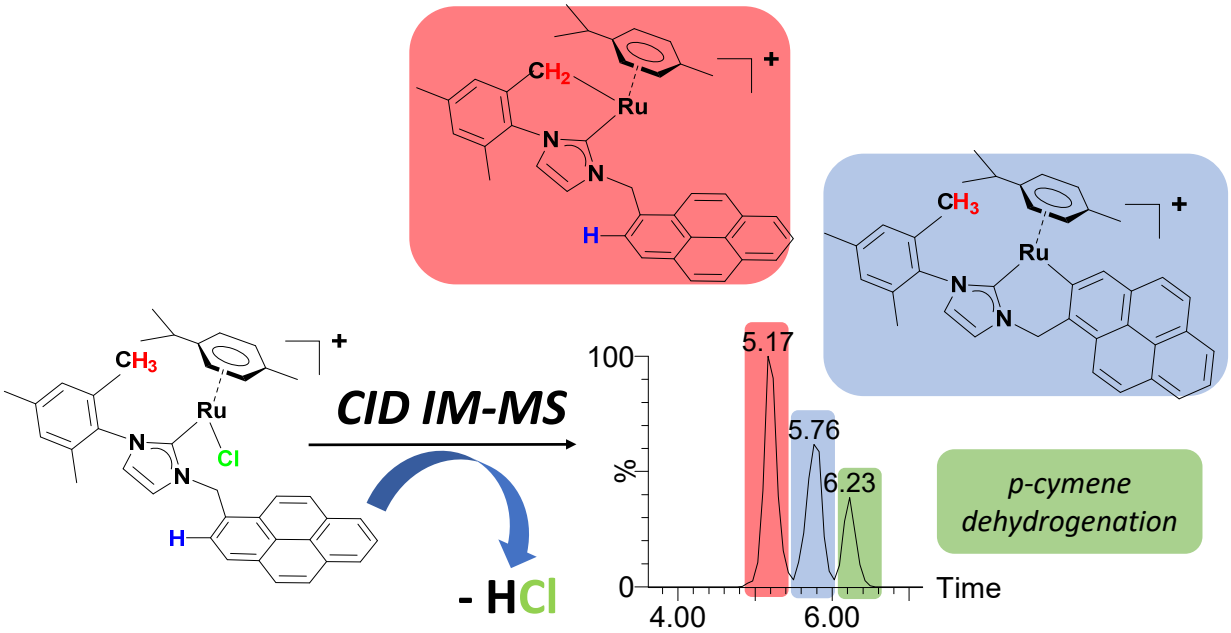

Ion Mobility Spectrometry Mass Spectrometry-based (IM-MS) approaches are presented to uncover site-selective C-H bond activation in a series of N-hetrocyclic carbene metal complexes based on the distinctive topology that the cyclometalated isomers adopt upon C-H bond activation.